

LafitE: Latent Diffusion Model with Feature Editing for Unsupervised Multi-class Anomaly Detection

Haonan Yin ^{1,*} Guanlong Jiao ^{1,*} Qianhui Wu ² Börje F. Karlsson ²

Biqing Huang ^{1,†} Chin-Yew Lin ²

¹Tsinghua University ²Microsoft Research Asia

yhn21, jgl22@mails.tsinghua.edu.cn hbq@tsinghua.edu.cn

qianhuiwu ,borjekar, cyl@microsoft.com

Abstract

In the context of flexible manufacturing systems that are required to produce different types and quantities of products with minimal reconfiguration, this paper addresses the problem of unsupervised multi-class anomaly detection: develop a unified model to detect anomalies from objects belonging to multiple classes when only normal data is accessible. We first explore the generative-based approach and investigate latent diffusion models for reconstruction to mitigate the notorious “identity shortcut” issue in auto-encoder based methods. We then introduce a feature editing strategy that modifies the input feature space of the diffusion model to further alleviate “identity shortcuts” and meanwhile improve the reconstruction quality of normal regions, leading to fewer false positive predictions. Moreover, we are the first who pose the problem of hyperparameter selection in unsupervised anomaly detection, and propose a solution of synthesizing anomaly data for a pseudo validation set to address this problem. Extensive experiments on benchmark datasets MVTec-AD and MPDD show that the proposed **LafitE**, i.e., **Latent Diffusion Model with Feature Editing**, outperforms state-of-art methods by a significant margin in terms of average AUROC. The hyperparameters selected via our pseudo validation set are well-matched to the real test set.

1. Introduction

Anomaly detection (AD) is the task of identifying and localizing anomalous patterns that are atypical of those seen in normal instances. It has attracted considerable attention from the research community in recent years for various application scenarios, such as industrial defect detection [5], medical image analysis [12], and video inspection [31]. However, there are significant difficulties in getting access

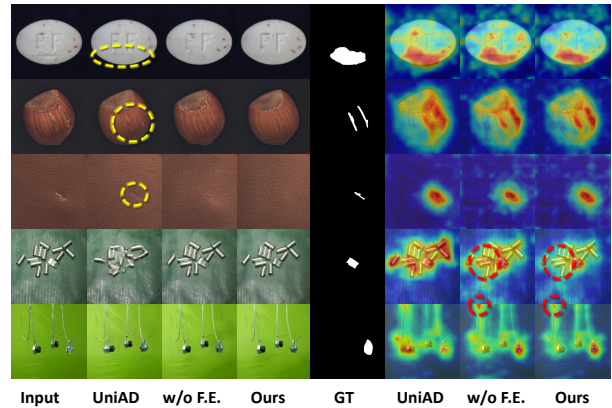


Figure 1: Visualization of the reconstructed images and the predicted heatmap of anomalous regions obtained from the baseline model UniAD and our approach. “GT”: the ground-true anomalous region. “w/o FE”: our approach without feature editing.

to a large number of anomalous data samples because the types of anomalies usually show great diversity in the real world, ranging from texture level (e.g., scratches and holes) to semantic level (e.g., missing components). Therefore, many works have been proposed for the extreme scenario, i.e., the *unsupervised* setting, where no prior information on anomalies is available and models need to be developed utilizing normal data only [6, 61, 58, 37, 9, 59, 8].

Flexible manufacturing systems are renowned for their ease of adapting to changes in product specifications and quantities, and are gaining increasing popularity for various benefits such as cost reduction, increased productivity, and shortened lead times. In such a context involving objects from multiple classes, most prior studies on unsupervised anomaly detection suggest training separate models for different classes [16, 55], which could be memory-intensive

* Equal Contribution Authors † Corresponding Authors

and rigid.

Recently, UniAD [59] proposed a unified model for unsupervised multi-class anomaly detection. It follows the **reconstruction** paradigm [61, 62, 55] and utilizes the Transformer architecture [52] as the backbone of the auto-encoder. The idea is that the auto-encoder trained on normal samples will produce low reconstruction error in normal regions but high reconstruction error in anomalous regions, hence allowing anomalies to be localized by the difference between an input sample and a reconstructed one. UniAD proposes three strategies to mitigate the “identity shortcut” issue, where the network may directly copy the input as the output regardless of whether it is normal or not, thus failing to localize the anomalies, *i.e.*, leading to false negative predictions. Though alleviating the problem, we can still observe the “identity shortcut” issue by visualizing their outputs as highlighted by yellow circles in Figure 1. We suggest the intrinsic nature of auto-encoder based methods, *i.e.*, aiming to learn a mapping function to the normal data manifold with no guarantee for anomalies to be mapped as well [61], makes it prone to errors.

To remedy this, we study the use of generative models for performing reconstruction while better learning the multi-class normal data distribution in the latent space. Diffusion models [15, 47, 35] have recently achieved great success in image generation with high guarantees of density estimation [19] and sampling quality [10]. We argue that using the diffusion model for anomaly reconstruction is a better paradigm in nature: The diffusion model learns the process from a Gaussian distribution to the normal distribution; The anomalous samples would be quite close to the normal ones on the near Gaussian manifold as illustrated in Figure 2 and Figure 5. In this way, they will have a higher probability to be reconstructed to normal samples via the denoising generation process of the diffusion model. Therefore, in this work, we take the diffusion model as the backbone of our proposed approach.

We propose **LafitE**, *i.e.*, **Latent Diffusion Model with Feature Editing**, to address unsupervised multi-class anomaly detection. Specifically, we first map input images into a latent feature space: We extract hierarchical patch representations using a model pre-trained on ImageNet, and produce a feature tensor for each image by aggregating multi-scale representations. With such aggregation, the feature slice corresponding to each position in the raw image contains both low-level texture information and high-level semantic information, which allows the method to deal with anomalies of various dimensions. Then, we employ a diffusion model [47] to reconstruct the aggregated feature tensor in the latent space. During inference, we first run the diffusion process to a maximum corruption step τ , and then perform the denoising process from the corrupted feature tensor for reconstruction. In view of the fact that patch rep-

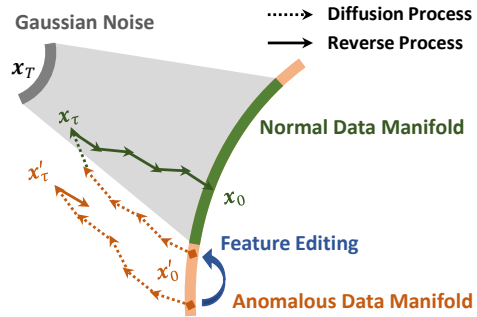


Figure 2: Illustration of how diffusion model and feature editing benefit the reconstruction. The diffusion process makes the normal and anomalous data less distinguishable in the near-Gaussian manifold, while feature editing further pulls the anomalous data closer to the normal data manifold in the input feature space.

resentations containing anomalous information may lead to corrupted feature tensors far from the normal data manifold (*e.g.*, x'_τ in Figure 2), we further propose a feature editing scheme over the *input space* of the diffusion model to pull patch representations corresponding to anomalies much closer to the normal data manifold. Particularly, we use a memory bank to store typical patch representations of seen normal data. During inference, we replace each patch representation of the feature tensor with its weighted nearest neighbors in the memory bank and perform reconstruction afterward with the learned diffusion model. Such feature editing brings benefits from two perspectives: i) Anomalous patch representations are directly dropped at the input stage of the reconstruction model and therefore the “identity shortcut” issue can be naturally mitigated. ii) The edited feature tensors locate much closer to the normal data manifold, which facilitates better reconstruction performance and thus reduces false positive predictions as highlighted by red circles in Figure 1.

Due to the inherent characteristics of unsupervised AD that only normal samples are available for learning, how to select hyperparameters for model training and inference becomes a critical issue but has not been well discussed in previous work. In this paper, we first pose the problem and further propose a simple but effective method to address it: We construct a pseudo validation set by leveraging the normal samples to synthesize anomalous samples. Experiments results indicate that the model’s performance on our pseudo validation set is generally consistent with that on the real test. The results also show that our LafitE significantly outperforms prior methods with a large margin in terms of average AUROC on both MVTec-AD and MPDD.

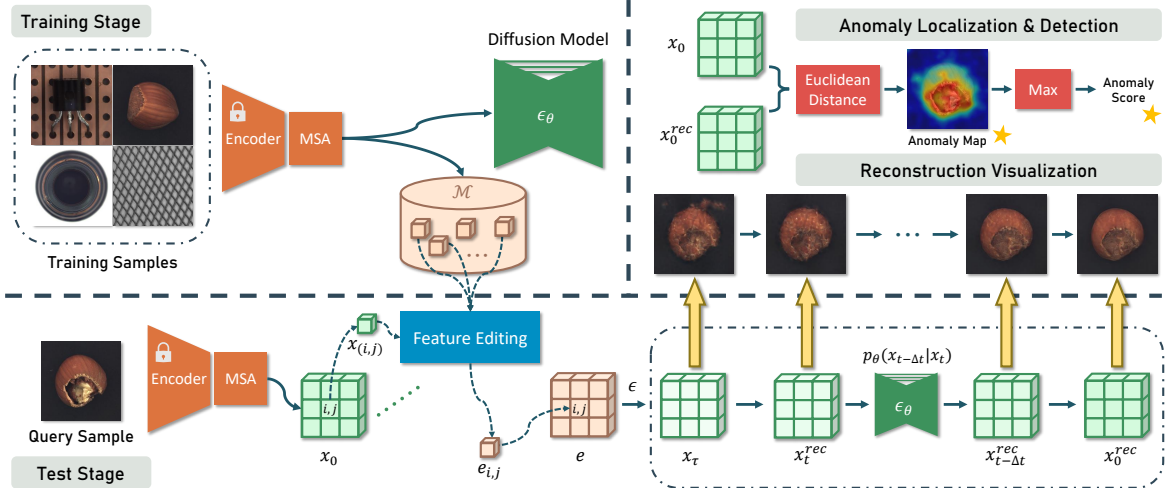


Figure 3: Overall framework of the proposed LafitE: It learns a diffusion model capable of modeling normal distribution during the training stage and stores a memory bank for feature editing. During the test stage, features of the query sample are first edited to ones closer to the normal data manifold. Then, the edited features are iteratively reconstructed via the denoising process of the diffusion model. Finally, anomaly localization and detection are performed by comparing the reconstructed features x_0^{rec} with the original features x_0 .

2. Related Work

Existing approaches for unsupervised anomaly detection and localization can be mainly divided into three categories: one-class classification based, feature embedding based, and reconstruction based.

One-class classification based methods build one-class classifiers from normal samples to distinguish them from anomalies. One-class support vector machine (OC-SVM) [45, 44] and support vector data description (SVDD) [51, 38, 39] are the most widely employed models for anomaly detection. Based on that, PatchSVDD [58] further splits an input image into patches and adopts self-supervised learning for anomaly localization.

Feature embedding based approaches generally consist of two steps, feature extraction and anomaly estimation [50]. For feature extraction, recent work [32, 34, 14] shows that using a network pre-trained on a large dataset like ImageNet [21] is effective for AD. For anomaly estimation, approaches like [7] compare deep feature embeddings of a target image and its K-nearest anomaly-free images. PatchCore [37] further introduces a memory bank for faster inference and reduced feature storage capacity. Others perform knowledge distillation to train a student model to estimate a scoring function [42, 9]. Moreover, normal samples are also modelled with Gaussian distribution or self-organizing maps (SOM) and anomaly scores computed based on Mahalanobis distance [8, 18, 23, 33].

Reconstruction based methods are developed based on the hypothesis that a model trained to reconstruct normal

samples only cannot correctly reconstruct anomalous samples [24, 64]. In this line of research, auto-encoder (AE) is one of the most widely used architecture for reconstruction [41, 4, 63, 46, 26]. Some work investigates the broader self-supervised learning paradigm for anomaly reconstruction [61, 22, 30, 62, 11]. UniAD [59] uses transformer as the backbone network and proposes a neighborhood mask encoder, a trainable query embedding, and a feature jittering strategy to address the shortcut issue. Multiple works also constraint the representation of latent space via memory banks [13, 28] and clustering [57]. Another prevalent methodology is based on generative models. Unlike auto-encoders that only consider the final reconstruction, generative model based studies aim to obtain the feature distribution of normal data. Since generative models only learn how to generate normal samples and thus the anomalous region can be localized using the discrepancy between the generated or constructed sample and the input [50]. Existing generative models for anomaly detection and localization primarily include variational auto-encoder (VAE) [24, 53, 20], generative adversarial network (GAN) [2, 43, 3, 40].

In this paper, we build our framework based on generative models for their superior reconstruction performance of normal samples [50] and take the diffusion model as backbone. The most related approaches to ours are [56, 29], which are also diffusion model based. However, both of them only target medical anomaly detection, while our approach considers more general cases ranging from texture level to semantic level. Moreover, [56] learns diffusion models at the image level and develops a multi-scale sim-

plex noise diffusion process to control the target anomaly size which is particularly critical in the medical domain. In contrast, our approach operates a latent diffusion model in the feature space for better scalability. Compared with [29], we additionally propose a memory bank based feature editing strategy to mitigate the shortcut issue of the latent diffusion model [35], and meanwhile, improve the reconstruction performance by pulling the initial state closer to the normal data manifold. Compared with other reconstruction based approaches with memory bank [13, 48], we produce the memory bank without training. Besides, we operate the memory bank at the input stage of the reconstruction model rather than the compressed latent vector space.

3. Method

In this section, we elaborate on the proposed LafitE. Figure 3 illustrates the overall framework.

3.1. Hierarchical Feature Extraction

Let $\mathcal{X}_N = \{\mathbf{X}_N^{(i)}\}_{i=1}^M$ denote the set of normal samples for training, where $\mathbf{X}_N^{(i)} \in \mathbb{R}^{H \times W \times C}$ is the i -th image. H , W , and C denote height, width, and channels, respectively. We use a pre-trained network as the image feature extractor and adopt a multi-scale aggregation (MSA) module to integrate hierarchical features of the input image.

Let ϕ denote a convolutional neural network with L levels. We first encode an image $\mathbf{X} \in \mathbb{R}^{H \times W \times C}$ into a set of feature representations $\phi(\mathbf{X}) = \{\phi_1(\mathbf{X}), \phi_2(\mathbf{X}), \dots, \phi_L(\mathbf{X})\}$, where $\phi_l(\mathbf{X}) \in \mathbb{R}^{h_l \times w_l \times c_l}$, $l \in [1, L]$. Considering that features from different layers correspond to different levels of information, *e.g.*, shallow layers contain more texture information and deep layers express semantic information, Here we select a subset of features $\mathcal{S}(\phi(\mathbf{X})) \subset \phi(\mathbf{X})$ and exclude the last layer to avoid the bias to the classification task for pre-training.

Then, we operate the MSA module: we perform feature alignment via an aggregation operation over $\mathcal{S}(\phi(\mathbf{X}))$. We scale features from different layers in $\mathcal{S}(\phi(\mathbf{X}))$ to a unified spatial dimension of height as h and width as w , and concatenate them along the channel axis with dimension c . Denote the resulted feature tensor as \mathbf{x} , we have:

$$\mathbf{x} = \text{Concat}(\{\text{Scale}(\phi_l(\mathbf{X}))\}), \quad \phi_l(\mathbf{X}) \in \mathcal{S}(\phi(\mathbf{X})). \quad (1)$$

Let $\mathbf{x}_{(i,j)} \in \mathbb{R}^c$ denote the feature slice at the position (i, j) of the aggregated feature tensor \mathbf{x} , it represents the dense multi-scale representations of corresponding patch-level regions. As the perceptual field of a patch embedding is usually large, the information contained in $\mathbf{x}_{(i,j)}$ may range from texture level to semantic level, thus benefiting the anomaly detection with various anomalous types in the multi-class setting.

3.2. Diffusion Model for Normal Feature Modeling

We utilize the denoising diffusion implicit model (DDIM) [47] in the latent space to model the compact distribution of normal samples. Given a feature tensor of a normal example, we aim to gradually corrupt it into Gaussian white noise by the noise addition process, *i.e.*, the diffusion process. Then, the network is trained to learn the score function of the normal distribution from Gaussian noise to normal feature tensors, which is called the denoising process, *a.k.a.*, the reverse process.

Following [15], we define the forward Markov diffusion process to generate images \mathbf{x}_t with noises of different scale from the input \mathbf{x}_0 :

$$q(\mathbf{x}_t | \mathbf{x}_{t-1}) = \mathcal{N}(\mathbf{x}_t; \sqrt{1 - \beta_t} \mathbf{x}_{t-1}, \beta_t \mathbf{I}), \quad (2)$$

where $0 < \beta_t < 1$ is the variance of noise level t , which can be also regarded as moment t . Larger t implies more noise. The marginal distribution of this Markov chain at moment t can be explicitly written as:

$$q(\mathbf{x}_t | \mathbf{x}_0) = \mathcal{N}(\mathbf{x}_t; \sqrt{\bar{\alpha}_t} \mathbf{x}_0, \sqrt{1 - \bar{\alpha}_t} \mathbf{I}), \quad (3)$$

with $\alpha_t = 1 - \beta_t$ and $\bar{\alpha}_t = \prod_{s=1}^t (1 - \beta_s)$.

To generate samples from Gaussian noise \mathbf{x}_T in the reverse processes, DDIM models the stepwise denoising prior probability as a Gaussian distribution as well:

$$p_\theta(\mathbf{x}_{t-1} | \mathbf{x}_t) = \mathcal{N}(\mathbf{x}_{t-1}; \mu_\theta(\mathbf{x}_t, t), \sigma_t^2 \mathbf{I}), \quad (4)$$

where σ_t is fixed for each t and the mean functions $\mu_\theta(\mathbf{x}_t, t)$ are trainable, which can be formulated as:

$$\mu_\theta(\mathbf{x}_t, t) = \frac{1}{\alpha_t} (\mathbf{x}_t - \frac{\beta_t}{\sqrt{1 - \bar{\alpha}_t}} \epsilon_\theta(\mathbf{x}_t, t)). \quad (5)$$

ϵ_θ is the noise function, (or score function), which can be predicted with the network parameterized by θ . Here we adopt U-net [36] as the network architecture, since its skip connections can effectively avoid irreversible information reduction brought by down-sampling in other CNN based auto-encoders. The training objective can be written as:

$$\mathcal{L}_\theta = \mathbb{E}_{\mathbf{x}, \epsilon} \|\epsilon - \epsilon_\theta(\sqrt{\bar{\alpha}_t} \mathbf{x}_0 + \sqrt{1 - \bar{\alpha}_t} \epsilon, t)\|_2^2, \quad (6)$$

where $\epsilon \sim \mathcal{N}(0, \mathbf{I})$.

Following DDIM [47], we perform iterative sampling in the denoising generation process via the following equation:

$$\begin{aligned} \mathbf{x}_{t-\Delta t} = & \sqrt{\bar{\alpha}_{t-\Delta t}} \left(\frac{\mathbf{x}_t - \sqrt{1 - \bar{\alpha}_t} \epsilon_\theta(\mathbf{x}_t, t)}{\bar{\alpha}_t} \right) \\ & + \sqrt{1 - \bar{\alpha}_{t-\Delta t} - \sigma_t^2} \epsilon_\theta(\mathbf{x}_t, t) + \sigma_t \mathbf{z}_t, \end{aligned} \quad (7)$$

with $\sigma_t = \eta \sqrt{(1 - \bar{\alpha}_{t-\Delta t}) / (1 - \bar{\alpha}_t)} \sqrt{1 - \bar{\alpha}_t / \bar{\alpha}_{t-\Delta t}}$, $\mathbf{z}_t \sim \mathcal{N}(0, \mathbf{I})$, and Δt denoting the sampling interval. With the trained diffusion model, we can generate the feature tensor of a normal sample from its corrupted noisy features by running the denoising process.

3.3. Reconstruction with Feature Editing

Diffusion Reconstruction We leverage the diffusion model as the backbone of the reconstruction framework. Instead of corrupting the original features into the Gaussian noise during the diffusion process, we pre-define a maximum corruption step $\tau \leq T$ to obtain the initial states for the reverse process during inference. In this way, the resulted \mathbf{x}_τ still keeps some information about the input \mathbf{x}_0 , and we can recursively sample from this partially noised sample for reconstruction. The corrupted feature tensor can be denoted as:

$$\mathbf{x}_\tau = \sqrt{\bar{\alpha}_\tau} \mathbf{x}_0 + \sqrt{1 - \bar{\alpha}_\tau} \epsilon. \quad (8)$$

Equation (8) shows that the initial state for reconstruction, *i.e.*, \mathbf{x}_τ inevitably contains the information in \mathbf{x}_0 . However, more information from \mathbf{x}_0 also means a higher possibility of identity-shortcut *w.r.t.* the anomalous regions. Therefore, we hope to find an appropriate τ , so that the corrupted \mathbf{x}_τ contains necessary information to reconstruct the normal regions in \mathbf{x}_0 , while the anomalous information is dispersed by the added noise.

Feature Editing We first build up a memory bank to preserve the representations of normal samples:

$$\mathcal{M} = \bigcup_{\mathbf{x} \in \mathcal{X}_N, i \in h, j \in w} \mathbf{x}_{(i,j)}. \quad (9)$$

Since the size of \mathcal{M} is proportional to that of the training data, we sample a core set \mathcal{M}_C from the whole memory bank \mathcal{M} with a greedy search algorithm[1] to diminish information redundancy, reduce storage space, and significantly improve inference speed.

Then, we edit each feature slice $\mathbf{x}_{(i,j)}^Q$ of a query sample \mathbf{x}^Q with a linear combination of its top-K nearest neighbors $\mathcal{N}_K(\mathbf{x}_{(i,j)}^Q) = \{\mathbf{n}_k\}_{k=1}^K$ in the core set \mathcal{M}_C :

$$\mathbf{e}_{i,j} = \sum_{k=1}^K \left(1 - \frac{\exp \|\mathbf{x}_{(i,j)}^Q - \mathbf{n}_k\|_2}{\sum_{\mathbf{n} \in \mathcal{N}_K(\mathbf{x}_{(i,j)}^Q)} \exp \|\mathbf{x}_{(i,j)}^Q - \mathbf{n}\|_2} \right) \cdot \mathbf{n}_k, \quad (10)$$

where $\mathbf{e}_{(i,j)}$ the edited feature slice *w.r.t.* at the position (i, j) and the whole feature tensor after editing can be denoted as \mathbf{e} . The weighting term for \mathbf{n}_k facilitate the edited feature tensor to integrate the information of similar, but different, normal patterns stored in \mathcal{M}_C , and meanwhile, taking into account the overall characteristics of normal data. More importantly, it also ensures that the distribution of edited features will not lie too far from the normal data manifold, which is conducive to the robustness of the method.

Note that we conduct the diffusion reconstruction on edited feature tensors \mathbf{e} , which excludes abnormal information in advance to address the identity shortcut issue.

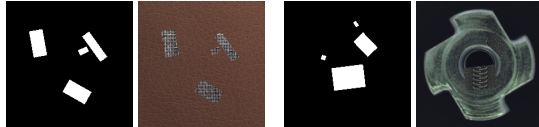


Figure 4: Masks and the synthesized anomalous samples.

More specifically, the initial state for reconstruction is derived from:

$$\mathbf{x}_\tau = \sqrt{\bar{\alpha}_\tau} \mathbf{e} + \sqrt{1 - \bar{\alpha}_\tau} \epsilon. \quad (11)$$

So far, the editing is independently conducted on each feature slice and do not consider the spatial correlation among different feature slices. Consequently, the joint distribution $p(\mathbf{e})$ has a certain distance from the normal feature distribution $p(\mathbf{x})$. Fortunately, applying a sufficient large noise on the edited feature in the diffusion process can make the manifold of \mathbf{e}_τ closer to that of \mathbf{x}_τ , which enables us to reconstruct higher quality features via the reverse or denoising process. Moreover, such reconstruction process considers the spatial correlation of feature slices in \mathbf{e} via the joint distribution $p(\mathbf{e}_\tau)$, which also contributes to better reconstruction performance.

Anomaly Estimation With the reconstructed features from the denoising process, we finally drive the feature-level anomaly score map by computing L2-norm reconstruction error between the denoised feature tensor \mathbf{x}_0^{rec} and the original \mathbf{x}_0 . Then we up-sample the score map with bilinear interpolation and apply Gaussian kernel smoothing to obtain the image-level score map for anomaly localization:

$$\mathbf{s} = \text{Upsample} (\|\mathbf{x}_0^{rec} - \mathbf{x}_0\|_2^2) * g_\sigma, \quad (12)$$

where $\mathbf{s} \in \mathbb{R}^{H \times W}$, g_σ denotes the Gaussian kernel with standard deviation of σ , and $*$ denotes the convolution operator. We perform average pooling on \mathbf{s} and take the maximum value as the final image-level anomaly score.

3.4. Anomalous Data Synthesis

Since normal samples are the only ones accessible in unsupervised anomaly detection, we found an absence of a validation set to guide the hyperparameter selection scheme. Such an issue caused by the intrinsic nature of the task has not been explored at either the concept level or experiment level in previous work. Inspired by CutPaste [22], we propose a straightforward method to synthesize anomaly samples and then build a pseudo validation set for hyperparameter selection.

Specifically, given a set of normal samples, we first initiate multiple masks of different shapes and sizes to ensure diversity. Then, we randomly rotate and combine these masks to produce a set of fragments from each normal sample. After that, we synthesize the anomaly sample by sticking these

extracted fragments to another randomly selected normal sample, and these fragments are labeled as anomalous regions. Figure 4 is the exemplification.

4. Experiment

4.1. Experimental Setup

Dataset. We conduct experiments on two widely used datasets, MVTEC-AD [5] and MPDD [17], to validate our approach. Both datasets have image-level labels and pixel-level annotations. MVTEC-AD consists of 3629 images for training and validation, and 1725 images for testing. The training set contains only normal images, while the test dataset contains both normal and anomalous images. There are 15 real-world categories in this dataset, including 5 classes of textures and 10 classes of objects, and each class has multiple types of defects. MPDD contains 6 classes of metal parts, focusing on defect detection during the fabrication of painted metal parts. Its training set is composed of 888 normal samples without defects, and the test set is composed of 458 samples either normal or anomalous. In particular, samples in MPDD have non-homogeneous backgrounds with diverse spatial orientations, different positions, and various light intensities, leading to greater challenges in anomaly detection.

Implementation Details. For experiments on both MVTEC-AD and MPDD, we use bi-linear interpolation to resize the images to 224×224 without any other enhancement. We adopt EfficientNet-b4 [49] pre-trained on ImageNet as ϕ in Section 3.1. Feature maps from stage 1 to stage 4 are resized to 32×32 for feature aggregation following UniAD [59]. We apply U-net [36] for ϵ_θ in the diffusion model. The base channel is set to 256 and channels multiple is set to (1, 2, 3, 4). We train the diffusion model for 1000 epochs on a single GPU (NVIDIA GeForce RTX 3090 24GB) with a batch size of 64, maximum time step T of 1000, and the cosine noise schedule [27]. Following UniAD [59], we use the AdamW optimizer [25] with weight decay 1×10^{-4} , the learning rate is set to 1×10^{-4} initially and dropped by 0.1 after 800 epochs. We use a keep rate of 10% to build the core set of the memory bank. Deviation for g_θ in Equation (12) is set to 4. For the setting of the corruption step τ and the number of neighbors K in Equation (10), please refer to Section 4.5. All results are reported from 5 random seeds.

4.2. Performance Comparison

In this section, we compare the proposed LafitE with various baseline models including one-class classification based PatchSVDD [58]; feature-embedding based PaDiM [8], RevDistill [9], DRAEM [61], and PatchCore [37]; auto-encoder based UniAD [59]; and generative model based

FastFlow [60]. Numbers for PatchSVDD [58], PaDiM [8], DRAEM [61], and UniAD [59] are copied from UniAD [59] for fair comparison. As for other results of MVTEC-AD and MPDD [17], we reproduced them in this work with publicly available implementations. Tables 1, 2, and 3 report the results of difference approaches on MVTEC-AD and MPDD for multi-class anomaly detection and localization, respectively. We can draw observations as follows.

The proposed LafitE surpasses previous state-of-the-art methods in both performance and robustness across various metrics and datasets with different levels of complexity. On MVTEC-AD, compared with UniAD, the previous state-of-the-art, our method obtains significant improvements of detection AUROC from 96.5% to 98.5% on average. LafitE also shows superiority over UniAD for localization AUROC with an average of 0.8%. On MPDD, our method outperforms RevDistill by 5.6% and 0.5% in terms of detection AUROC and localization AUROC, respectively. This well demonstrates the effectiveness of the proposed approach. Considering that the amount of normal and abnormal samples are often unbalanced in real application scenarios, the metric AU-PR was exploited to have a fairer view on performance evaluation [65]. Thus we also evaluate AU-PR on both datasets here and Table 3 shows the results. Generally speaking, LafitE achieves superior performance. Though the performance of PatchCore on MVTEC-AD anomaly localization looks promising, it drops dramatically on MPDD, where the normal samples are more complicated. By comparison, our approach demonstrates more robustness.

Our method demonstrates less bias to the category of objects and leads to more consistent performance from anomaly detection to anomaly localization. As shown in Table 1 and 2, though prior methods such as RevDistill [9], PatchCore [37], FastFlow [60], and UniAD [59] achieve promising averaged performance across all classes, their inter-category standard variation is much larger than ours with a maximum gap of 11.53, highlighting the consistency of our approach for multi-class anomaly detection. Table 1 and 2 also indicate that unlike RevDistill [9] and PatchCore [37] producing excellent performance for localization but resulting in unsatisfied results for detection, our model achieves the best averaged performance for both detection and localization.

Reconstruction based approaches such as LafitE and UniAD [59] generally lead to superior detection performance than feature embedding based approaches like RevDistill [9] and PatchCore [37]. We conjecture this is because feature editing based methods focus more on local patches while the nature of reconstruction makes the reconstruction based approaches gain a global view of inputs. This awareness of the relationship among adjacent patches enhances the ability to deal with image level detection.

Table 1: AUROC scores of multi-class anomaly **detection** and **localization** (shown as Det. / Loc.) on MVTec-AD [5]. We highlight the highest results in color and underline the results lower than 80.0%.

Category	PatchSVDD [58]	PaDiM [8]	DRAEM [61]	RevDistill [9]	PatchCore [37]	FastFlow [60]	UniAD [59]	LafitE (ours)
Bottle	85.5 / 87.6	97.9 / 96.1	97.5 / 87.6	46.2 / 95.5	97.5 / 98.1	97.6 / 84.9	99.7 / 98.1	100 ± 0.00 / 98.4 ± 0.01
Cable	64.4 / 62.2	70.9 / 81.0	57.8 / 71.3	76.9 / 83.4	99.7 / 98.1	97.9 / 97.4	95.2 / 97.3	97.2 ± 0.25 / 97.3 ± 0.07
Capsule	61.3 / 83.1	73.4 / 96.9	65.3 / 50.5	97.3 / 98.5	78.0 / 97.6	95.6 / 98.7	86.9 / 98.5	96.8 ± 0.25 / 98.9 ± 0.01
Hazelnut	83.9 / 97.4	85.5 / 96.3	93.7 / 96.9	100 / 98.9	100 / 98.4	98.2 / 99.0	99.8 / 98.1	100 ± 0.00 / 98.4 ± 0.05
Metal Nut	80.9 / 96.0	88.0 / 84.8	72.8 / 62.2	94.9 / 93.4	98.6 / 98.5	98.2 / 97.7	99.2 / 94.8	99.8 ± 0.06 / 96.8 ± 0.01
Pill	89.4 / 96.5	68.8 / 87.7	82.2 / 94.4	94.9 / 98.3	94.8 / 97.6	95.0 / 98.7	93.7 / 95.0	98.0 ± 0.16 / 96.7 ± 0.03
Screw	80.9 / 74.3	56.9 / 94.1	92.0 / 95.5	96.5 / 99.4	72.0 / 96.5	79.6 / 98.3	87.5 / 98.3	95.4 ± 0.28 / 99.5 ± 0.01
Toothbrush	99.4 / 98.0	95.3 / 95.6	90.6 / 97.7	83.6 / 98.9	98.3 / 98.6	81.9 / 98.7	94.2 / 98.4	92.9 ± 0.22 / 98.8 ± 0.00
Transistor	77.5 / 78.5	86.6 / 92.3	74.8 / 64.5	91.5 / 87.2	99.6 / 97.3	91.4 / 94.7	99.8 / 97.9	99.6 ± 0.10 / 97.4 ± 0.02
Zipper	77.8 / 95.1	79.7 / 94.8	98.8 / 98.3	98.9 / 98.1	95.9 / 97.5	95.4 / 97.9	95.8 / 96.8	99.4 ± 0.09 / 98.3 ± 0.02
Carpet	63.3 / 78.6	93.8 / 97.6	98.0 / 98.6	95.7 / 98.7	96.8 / 98.7	99.6 / 94.0	99.8 / 98.5	99.8 ± 0.05 / 98.7 ± 0.03
Grid	66.0 / 70.8	73.9 / 71.0	99.3 / 98.7	97.9 / 99.2	82.6 / 96.6	91.1 / 96.3	98.2 / 96.5	99.9 ± 0.03 / 98.5 ± 0.01
Leather	60.8 / 93.5	99.9 / 84.8	98.7 / 97.3	100 / 99.3	100 / 99.0	95.8 / 92.6	100 / 98.8	100 ± 0.00 / 99.2 ± 0.02
Tile	88.3 / 92.1	93.3 / 80.5	99.8 / 98.0	97.7 / 95.8	98.4 / 94.8	99.8 / 93.5	99.3 / 91.8	100 ± 0.00 / 93.2 ± 0.04
Wood	72.1 / 80.7	98.4 / 89.1	99.8 / 96.0	98.9 / 95.8	97.1 / 93.8	98.3 / 91.8	98.6 / 93.2	98.7 ± 0.18 / 94.3 ± 0.15
Average	76.8 / 85.6	84.2 / 89.5	88.1 / 87.2	91.4 / 96.0	94.0 / 97.4	94.4 / 95.6	96.5 / 96.8	98.5 ± 0.03 / 97.6 ± 0.02
Inter-category Std	11.35 / 11.14	12.54 / 7.56	13.54 / 16.36	13.57 / 4.75	8.56 / 1.42	5.90 / 3.72	4.21 / 2.12	2.04 / 1.73

Table 2: AUROC scores of multi-class anomaly **detection** and **localization** (shown as Det. / Loc.) on MPDD [17]. We highlight the highest results in color and underline the results lower than 80.0%.

Category	PatchSVDD [58]	PaDiM [8]	DRAEM [61]	RevDistill [9]	PatchCore [37]	FastFlow [60]	UniAD [59]	LafitE (ours)
Bracket Black	85.8 / 67.9	71.1 / 93.1	81.2 / 97.9	81.0 / 97.3	77.3 / 96.9	81.4 / 82.4	96.8 / 94.9	98.5 ± 0.12 / 99.3 ± 0.02
Bracket Brown	97.3 / 63.2	75.0 / 95.0	85.0 / 53.8	86.0 / 97.2	83.1 / 95.3	97.5 / 80.3	98.9 / 98.6	96.5 ± 0.39 / 99.5 ± 0.01
Bracket White	87.2 / 55.8	73.0 / 97.2	78.8 / 95.7	83.6 / 98.8	75.8 / 99.6	72.3 / 98.1	88.7 / 96.0	92.4 ± 0.39 / 98.4 ± 0.01
Connector	99.8 / 90.2	83.8 / 97.2	88.8 / 85.1	99.5 / 99.5	96.4 / 98.4	94.0 / 94.0	91.0 / 98.0	96.7 ± 0.23 / 99.1 ± 0.02
Metal Plate	84.6 / 91.0	51.1 / 90.2	100 / 99.2	100 / 99.2	100 / 98.6	99.7 / 97.9	73.0 / 94.0	100 ± 0.00 / 98.7 ± 0.01
Tubes	79.1 / 41.7	75.6 / 88.7	96.2 / 98.2	95.5 / 99.1	68.5 / 97.3	77.1 / 96.9	76.9 / 92.3	94.8 ± 0.46 / 99.2 ± 0.01
Average	89.0 / 68.3	71.6 / 93.6	88.3 / 88.3	90.9 / 98.5	83.5 / 97.7	87.0 / 91.6	87.5 / 95.6	96.5 ± 0.08 / 99.0 ± 0.01
Inter-category Std	7.26 / 17.72	9.99 / 3.26	7.66 / 16.14	7.67 / 0.92	11.28 / 1.38	10.52 / 7.40	9.59 / 2.19	2.44 / 0.36

Table 3: Averaged AU-PR on MVTec-AD [5] and MPDD [17]. Best results are in bold.

Method	MVTec-AD		MPDD	
	Det.	Loc.	Det.	Loc.
RevDistill	95.3	50.1	92.3	41.6
PatchCore	98.2	54.3	90.4	36.8
FastFlow	97.0	42.6	80.1	27.8
UniAD	98.9	44.8	89.8	20.3
LafitE (ours)	99.4 ± 0.02	51.3 ± 0.16	94.8 ± 0.03	44.9 ± 0.22

4.3. Ablation Study

Here we validate the contributions of different components in the proposed LafitE. We introduce two variants: i) *LafitE w/o F.E.*, which removes the feature editing strategy from the proposed LafitE and directly leverages the latent diffusion model for anomaly detection. ii) *UniAD w/ F.E.*, where we replace the diffusion model in LafitE with UniAD for reconstruction. Table 4 highlights the results.

Comparing LafitE with *LafitE w/o F.E.*, we can see that incorporating the proposed feature editing strategy brings

Table 4: Ablation results of averaged AUROC on MVTec-AD and MPDD. LDM denotes the latent diffusion model based backbone. F.E. denotes the feature editing strategy.

	Method	Architecture	F.E.	Detection	Localization
MVTec-AD	LafitE	LDM	✓	98.5	97.6
	LafitE w/o F.E.	LDM	✗	98.2	97.4
	UniAD w/ F.E.	Transformer	✓	96.8	97.1
	UniAD	Transformer	✗	96.5	96.8
MPDD	LafitE	LDM	✓	96.5	99.0
	LafitE w/o F.E.	LDM	✗	93.6	98.3
	UniAD w/ F.E.	Transformer	✓	86.6	95.6
	UniAD	Transformer	✗	87.5	95.6

consistent performance gain to the basic construction model on both datasets, well verifying its effectiveness. Table 4 also shows that LafitE outperforms *UniAD w/ F.E.* and *LafitE w/o F.E.* outperforms UniAD. This highlights the superiority of the proposed generative model based approach over the auto-encoder framework in UniAD.

We further visualize the reconstructed images by UniAD, *LafitE w/o F.E.*, and LafitE for more in-depth un-

derstanding. As shown in Figure 1, though UniAD well reconstructs normal regions, anomalous information is still kept in the reconstructed image, thus hurting the distinguishability between normal regions and anomalous regions for anomaly detection. In contrast, our LafitE and *LafitE w/o F.E.* exhibit much less identity shortcut issues in anomalous regions. Figure 1 also depicts that compared with *LafitE w/o F.E.*, LafitE not only produces larger discrepancy in anomalous regions after reconstruction which alleviates the identity shortcut issue, but also leads to lower reconstruction error in normal regions which helps reduce the false positive predictions. This implies that the proposed feature editing strategy can benefit the diffusion model with the corrupted states getting closer to the normal data manifold, well verifying our motivation.

4.4. Feature Distribution in Diffusion Process

To better understand the change of feature distribution *w.r.t.* both normal samples and abnormal samples at different diffusion step τ , here we use PCA [54] for dimension reduction and visualize the data points from MVTEC-AD (Wood) as in Figure 5. We can see that anomalies are closer and less distinguishable from normal ones in the near-Gaussian manifold (Figure 5b) than in the original data manifold (Figure 5a). Therefore, when conducting the denoising generation process of the diffusion model from the near-Gaussian manifold, anomalous samples will have a high probability to be reconstructed into normal samples, which proves the rationality of our motivation to explore the diffusion model as the backbone to mitigate the identity shortcut issue in reconstruction.

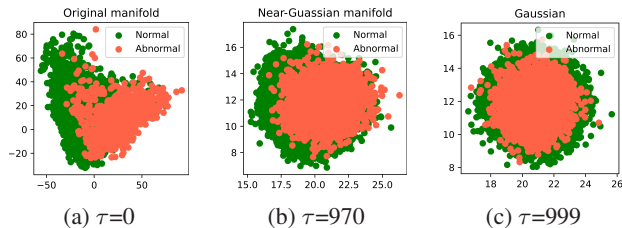


Figure 5: Distribution of both normal and abnormal features at different diffusion step τ .

4.5. Evaluation of Hyperparameter Selection

Here we study the effectiveness of the proposed strategy that synthesizes anomaly samples to construct a pseudo validation set for hyperparameter selection (Section 3.4). It is expected that the best parameters selected via the constructed validation set can also lead to the best performance on the real test set. Specifically, we carry out the hyperparameter selection before inference and consider two hyperparameters: the corruption steps τ of the latent diffusion

model and the number of neighbors K used for feature editing. We begin by using the model *LafitE w/o F.E.* to identify a τ that yields the highest detection AUROC on the pseudo validation set. Next, we fix the selected τ and repeat this approach to identify the value of K using the LafitE model.

Figure 6 depicts the detection AUROC obtained from different hyperparameters on both the constructed pseudo validation set and the test set of MVTEC-AD [5]. Though the gap between the performance curves obtained from the pseudo validation set and the test set suggests the potential improvement of the pseudo validation set, what is satisfying is that both curves demonstrate similar trends. More importantly, the hyperparameters along with the best performance on the pseudo validation set also achieve the highest AUROC score on the test set, which ensures that the unsupervised model can perform well in the test phase.

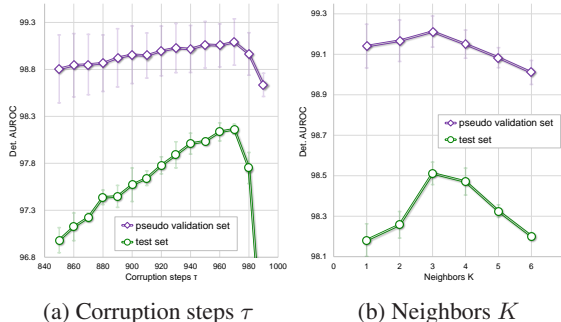


Figure 6: Analysis of the hyperparameter selection strategy.

5. Conclusion

In this work, we propose an effective framework for unsupervised multi-class anomaly detection: **LafitE**, *i.e.*, **Latent Diffusion Model with Feature Editing**. It mainly involves a diffusion model to learn the distribution of normal features and a feature editing strategy to pull the anomalous data toward the normal data manifold, both eliminating the identity shortcut issue in most reconstruction based methods. We also highlight the problem of hyperparameter selection in the unsupervised anomaly detection task which is not discussed in prior works. We emphasize the commonly overlooked challenge of hyperparameter selection in the unsupervised anomaly detection task and propose a strategy to construct a pseudo validation set by synthesizing anomalous samples. We evaluate the proposed LafitE on MVTEC-AD and MPDD datasets. Experimental results show that our method achieves the SOTA performance on both anomaly detection and anomaly localization. The qualitative analysis and ablation study demonstrate that the proposed LafitE outperforms the baseline method in solving the identity shortcut issue and our feature editing module can also bring benefits in reducing inaccurate reconstruction.

References

- [1] Pankaj K Agarwal et al. Geometric approximation via coresets. *Combinatorial and computational geometry*, 2005. 5
- [2] Samet Akcay, Amir Atapour-Abarghouei, and Toby P Breckon. Ganomaly: Semi-supervised anomaly detection via adversarial training. In *Asian conference on computer vision*, pages 622–637. Springer, 2018. 3
- [3] Christoph Baur, Robert Graf, Benedikt Wiestler, Shadi Albarqouni, and Nassir Navab. Steganomaly: Inhibiting cyclegan steganography for unsupervised anomaly detection in brain mri. In *International conference on medical image computing and computer-assisted intervention*, pages 718–727. Springer, 2020. 3
- [4] Christoph Baur, Benedikt Wiestler, Shadi Albarqouni, and Nassir Navab. Deep autoencoding models for unsupervised anomaly segmentation in brain mr images. In *International MICCAI brainlesion workshop*, pages 161–169. Springer, 2018. 3
- [5] Paul Bergmann, Michael Fauser, David Sattlegger, and Carsten Steger. Mytec ad—a comprehensive real-world dataset for unsupervised anomaly detection. In *Proceedings of the IEEE/CVF conference on computer vision and pattern recognition*, pages 9592–9600, 2019. 1, 6, 7, 8
- [6] Paul Bergmann, Michael Fauser, David Sattlegger, and Carsten Steger. Uninformed students: Student-teacher anomaly detection with discriminative latent embeddings. *2020 IEEE/CVF Conference on Computer Vision and Pattern Recognition (CVPR)*, pages 4182–4191, 2020. 1
- [7] Niv Cohen and Yedid Hoshen. Sub-image anomaly detection with deep pyramid correspondences. *arXiv preprint arXiv:2005.02357*, 2020. 3
- [8] Thomas Defard, Aleksandr Setkov, Angélique Loesch, and Romaric Audigier. Padim: a patch distribution modeling framework for anomaly detection and localization. In *International Conference on Pattern Recognition*, pages 475–489. Springer, 2021. 1, 3, 6, 7
- [9] Hanqiu Deng and Xingyu Li. Anomaly detection via reverse distillation from one-class embedding. In *Proceedings of the IEEE/CVF Conference on Computer Vision and Pattern Recognition*, pages 9737–9746, 2022. 1, 3, 6, 7
- [10] Prafulla Dhariwal and Alex Nichol. Diffusion models beat gans on image synthesis. *ArXiv*, abs/2105.05233, 2021. 2
- [11] Ye Fei, Chaoqin Huang, Cao Jinkun, Maosen Li, Ya Zhang, and Cewu Lu. Attribute restoration framework for anomaly detection. *IEEE Transactions on Multimedia*, 2020. 3
- [12] Tharindu Fernando, Harshala Gammulle, Simon Denman, Sridha Sridharan, and Clinton Fookes. Deep learning for medical anomaly detection—a survey. *ACM Computing Surveys (CSUR)*, 54(7):1–37, 2021. 1
- [13] Dong Gong, Lingqiao Liu, Vuong Le, Budhaditya Saha, Moussa Reda Mansour, Svetha Venkatesh, and Anton van den Hengel. Memorizing normality to detect anomaly: Memory-augmented deep autoencoder for unsupervised anomaly detection. In *Proceedings of the IEEE/CVF International Conference on Computer Vision*, pages 1705–1714, 2019. 3, 4
- [14] Dan Hendrycks, Kimin Lee, and Mantas Mazeika. Using pre-training can improve model robustness and uncertainty. In *International Conference on Machine Learning*, pages 2712–2721. PMLR, 2019. 3
- [15] Jonathan Ho, Ajay Jain, and Pieter Abbeel. Denoising diffusion probabilistic models. *Advances in Neural Information Processing Systems*, 33:6840–6851, 2020. 2, 4
- [16] Chaoqin Huang, Haoyan Guan, Aofan Jiang, Ya Zhang, Michael Spratling, and Yan-Feng Wang. Registration based few-shot anomaly detection. In *Computer Vision—ECCV 2022: 17th European Conference, Tel Aviv, Israel, October 23–27, 2022, Proceedings, Part XXIV*, pages 303–319. Springer, 2022. 1
- [17] Stepan Jezek, Martin Jonák, Radim Burget, Pavel Dvorak, and Milos Skotak. Deep learning-based defect detection of metal parts: evaluating current methods in complex conditions. *2021 13th International Congress on Ultra Modern Telecommunications and Control Systems and Workshops (ICUMT)*, pages 66–71, 2021. 6, 7
- [18] Jin-Hwa Kim, Do-Hyeong Kim, Saehoon Yi, and Taehoon Lee. Semi-orthogonal embedding for efficient unsupervised anomaly segmentation. *ArXiv*, abs/2105.14737, 2021. 3
- [19] Diederik P. Kingma, Tim Salimans, Ben Poole, and Jonathan Ho. Variational diffusion models. *ArXiv*, abs/2107.00630, 2021. 2
- [20] Nejc Kozamernik and Drago Bračun. Visual inspection system for anomaly detection on ktl coatings using variational autoencoders. *Procedia CIRP*, 93:1558–1563, 2020. 3
- [21] Alex Krizhevsky, Ilya Sutskever, and Geoffrey E Hinton. Imagenet classification with deep convolutional neural networks. *Communications of the ACM*, 60(6):84–90, 2017. 3
- [22] Chun-Liang Li, Kihyuk Sohn, Jinsung Yoon, and Tomas Pfister. Cutpaste: Self-supervised learning for anomaly detection and localization. In *Proceedings of the IEEE/CVF Conference on Computer Vision and Pattern Recognition*, pages 9664–9674, 2021. 3, 5
- [23] Ning Li, Kaitao Jiang, Zhiheng Ma, Xing Wei, Xiaopeng Hong, and Yihong Gong. Anomaly detection via self-organizing map. In *2021 IEEE International Conference on Image Processing (ICIP)*, pages 974–978. IEEE, 2021. 3
- [24] Wenqian Liu, Runze Li, Meng Zheng, Srikrishna Karanam, Ziyang Wu, Bir Bhanu, Richard J Radke, and Octavia Camps. Towards visually explaining variational autoencoders. In *Proceedings of the IEEE/CVF Conference on Computer Vision and Pattern Recognition*, pages 8642–8651, 2020. 3
- [25] Ilya Loshchilov and Frank Hutter. Decoupled weight decay regularization. *arXiv preprint arXiv:1711.05101*, 2017. 6
- [26] Pankaj Mishra, Riccardo Verk, Daniele Fornasier, Claudio Picciarelli, and Gian Luca Foresti. Vt-adl: A vision transformer network for image anomaly detection and localization. In *2021 IEEE 30th International Symposium on Industrial Electronics (ISIE)*, pages 01–06. IEEE, 2021. 3
- [27] Alexander Quinn Nichol and Prafulla Dhariwal. Improved denoising diffusion probabilistic models. In *International Conference on Machine Learning*, pages 8162–8171. PMLR, 2021. 6

- [28] Tongzhi Niu, Bin Li, Weifeng Li, Yuanhong Qiu, and Shuanlong Niu. Positive-sample-based surface defect detection using memory-augmented adversarial autoencoders. *IEEE/ASME Transactions on Mechatronics*, 27(1):46–57, 2022. 3
- [29] Walter Hugo Lopez Pinaya, Mark S. Graham, Robert Gray, Pedro F. Da Costa, Petru-Daniel Tudosiu, Paul Wright, Yee-Haur Mah, Andrew D. Mackinnon, James Teo, Hans Rolf Jäger, David John Werring, Geraint Rees, Parashkev Nachev, Sébastien Ourselin, and Manuel Jorge Cardoso. Fast unsupervised brain anomaly detection and segmentation with diffusion models. In *MICCAI*, 2022. 3, 4
- [30] Jonathan Pirnay and Keng Chai. Inpainting transformer for anomaly detection. In *International Conference on Image Analysis and Processing*, pages 394–406. Springer, 2022. 3
- [31] Bharathkumar Ramachandra, Michael Jones, and Ranga Raju Vatsavai. A survey of single-scene video anomaly detection. *IEEE transactions on pattern analysis and machine intelligence*, 2020. 1
- [32] Tal Reiss, Niv Cohen, Liron Bergman, and Yedid Hoshen. Panda: Adapting pretrained features for anomaly detection and segmentation. In *Proceedings of the IEEE/CVF Conference on Computer Vision and Pattern Recognition*, pages 2806–2814, 2021. 3
- [33] Oliver Rippel, Arnav Chavan, Chucai Lei, and Dorit Merhof. Transfer learning gaussian anomaly detection by fine-tuning representations. *Proceedings of the 2nd International Conference on Image Processing and Vision Engineering*, 2021. 3
- [34] Oliver Rippel, Patrick Mertens, and Dorit Merhof. Modeling the distribution of normal data in pre-trained deep features for anomaly detection. In *2020 25th International Conference on Pattern Recognition (ICPR)*, pages 6726–6733. IEEE, 2021. 3
- [35] Robin Rombach, A. Blattmann, Dominik Lorenz, Patrick Esser, and Björn Ommer. High-resolution image synthesis with latent diffusion models. *2022 IEEE/CVF Conference on Computer Vision and Pattern Recognition (CVPR)*, pages 10674–10685, 2022. 2, 4
- [36] Olaf Ronneberger, Philipp Fischer, and Thomas Brox. U-net: Convolutional networks for biomedical image segmentation. In *International Conference on Medical image computing and computer-assisted intervention*, pages 234–241. Springer, 2015. 4, 6
- [37] Karsten Roth, Latha Pemula, Joaquin Zepeda, Bernhard Schölkopf, Thomas Brox, and Peter Gehler. Towards total recall in industrial anomaly detection. In *Proceedings of the IEEE/CVF Conference on Computer Vision and Pattern Recognition*, pages 14318–14328, 2022. 1, 3, 6, 7
- [38] Lukas Ruff, Robert Vandermeulen, Nico Goernitz, Lucas Deecker, Shoaib Ahmed Siddiqui, Alexander Binder, Emmanuel Müller, and Marius Kloft. Deep one-class classification. In *International conference on machine learning*, pages 4393–4402. PMLR, 2018. 3
- [39] Lukas Ruff, Robert A Vandermeulen, Nico Görnitz, Alexander Binder, Emmanuel Müller, Klaus-Robert Müller, and Marius Kloft. Deep semi-supervised anomaly detection. *arXiv preprint arXiv:1906.02694*, 2019. 3
- [40] Mohammad Sabokrou, Mohammad Khaloeei, Mahmood Fathy, and Ehsan Adeli. Adversarially learned one-class classifier for novelty detection. In *Proceedings of the IEEE conference on computer vision and pattern recognition*, pages 3379–3388, 2018. 3
- [41] Mayu Sakurada and Takehisa Yairi. Anomaly detection using autoencoders with nonlinear dimensionality reduction. In *Proceedings of the MLSDA 2014 2nd workshop on machine learning for sensory data analysis*, pages 4–11, 2014. 3
- [42] Mohammadreza Salehi, Niousha Sadjadi, Soroosh Baselizadeh, Mohammad Hossein Rohban, and Hamid R. Rabiee. Multiresolution knowledge distillation for anomaly detection. *2021 IEEE/CVF Conference on Computer Vision and Pattern Recognition (CVPR)*, pages 14897–14907, 2021. 3
- [43] Thomas Schlegl, Philipp Seeböck, Sebastian M Waldstein, Georg Langs, and Ursula Schmidt-Erfurth. f-anogan: Fast unsupervised anomaly detection with generative adversarial networks. *Medical image analysis*, 54:30–44, 2019. 3
- [44] Bernhard Schölkopf, John C Platt, John Shawe-Taylor, Alex J Smola, and Robert C Williamson. Estimating the support of a high-dimensional distribution. *Neural computation*, 13(7):1443–1471, 2001. 3
- [45] Bernhard Schölkopf, Robert C Williamson, Alex Smola, John Shawe-Taylor, and John Platt. Support vector method for novelty detection. *Advances in neural information processing systems*, 12, 1999. 3
- [46] Yong Shi, Jie Yang, and Zhiqian Qi. Unsupervised anomaly segmentation via deep feature reconstruction. *Neurocomputing*, 424:9–22, 2021. 3
- [47] Jiaming Song, Chenlin Meng, and Stefano Ermon. Denoising diffusion implicit models. *arXiv preprint arXiv:2010.02502*, 2020. 2, 4
- [48] Daniel Stanley Tan, Yi-Chun Chen, Trista Pei-Chun Chen, and Wei-Chao Chen. Trustmae: A noise-resilient defect classification framework using memory-augmented autoencoders with trust regions. In *Proceedings of the IEEE/CVF winter conference on applications of computer vision*, pages 276–285, 2021. 4
- [49] Mingxing Tan and Quoc Le. Efficientnet: Rethinking model scaling for convolutional neural networks. In *International conference on machine learning*, pages 6105–6114. PMLR, 2019. 6
- [50] Xian Tao, Xinyi Gong, Xin Yu Zhang, Shaohua Yan, and Chandranath Adak. Deep learning for unsupervised anomaly localization in industrial images: A survey. *IEEE Transactions on Instrumentation and Measurement*, 71:1–21, 2022. 3
- [51] David MJ Tax and Robert PW Duin. Support vector data description. *Machine learning*, 54(1):45–66, 2004. 3
- [52] Ashish Vaswani, Noam Shazeer, Niki Parmar, Jakob Uszkoreit, Llion Jones, Aidan N Gomez, Łukasz Kaiser, and Illia Polosukhin. Attention is all you need. *Advances in neural information processing systems*, 30, 2017. 2
- [53] Shashanka Venkataramanan, Kuan-Chuan Peng, Rajat Vikram Singh, and Abhijit Mahalanobis. Attention guided anomaly localization in images. In *European*

- Conference on Computer Vision*, pages 485–503. Springer, 2020. 3
- [54] Svante Wold, Kim Esbensen, and Paul Geladi. Principal component analysis. *Chemometrics and intelligent laboratory systems*, 2(1-3):37–52, 1987. 8
- [55] Jih-Ciang Wu, Ding-Jie Chen, Chiou-Shann Fuh, and Tyng-Luh Liu. Learning unsupervised metaformer for anomaly detection. In *Proceedings of the IEEE/CVF International Conference on Computer Vision*, pages 4369–4378, 2021. 1, 2
- [56] Julian Wyatt, Adam Leach, Sebastian M. Schmon, and Chris G. Willcocks. Anoddpn: Anomaly detection with denoising diffusion probabilistic models using simplex noise. *2022 IEEE/CVF Conference on Computer Vision and Pattern Recognition Workshops (CVPRW)*, pages 649–655, 2022. 3
- [57] Hua Yang, Yifan Chen, Kaiyou Song, and Zhouping Yin. Multiscale feature-clustering-based fully convolutional autoencoder for fast accurate visual inspection of texture surface defects. *IEEE Transactions on Automation Science and Engineering*, 16(3):1450–1467, 2019. 3
- [58] Jihun Yi and Sungroh Yoon. Patch svdd: Patch-level svdd for anomaly detection and segmentation. In *Proceedings of the Asian Conference on Computer Vision*, 2020. 1, 3, 6, 7
- [59] Zhiyuan You, Lei Cui, Yujun Shen, Kai Yang, Xin Lu, Yu Zheng, and Xinyi Le. A unified model for multi-class anomaly detection. *Advances in Neural Information Processing Systems*, 2022. 1, 2, 3, 6, 7
- [60] Jiawei Yu, Ye Zheng, Xiang Wang, Wei Li, Yushuang Wu, Rui Zhao, and Liwei Wu. Fastflow: Unsupervised anomaly detection and localization via 2d normalizing flows. *arXiv preprint arXiv:2111.07677*, 2021. 6, 7
- [61] Vitjan Zavrtanik, Matej Kristan, and Danijel Skočaj. Draema discriminatively trained reconstruction embedding for surface anomaly detection. In *Proceedings of the IEEE/CVF International Conference on Computer Vision*, pages 8330–8339, 2021. 1, 2, 3, 6, 7
- [62] Vitjan Zavrtanik, Matej Kristan, and Danijel Skočaj. Reconstruction by inpainting for visual anomaly detection. *Pattern Recognition*, 112:107706, 2021. 2, 3
- [63] Yiru Zhao, Bing Deng, Chen Shen, Yao Liu, Hongtao Lu, and Xian-Sheng Hua. Spatio-temporal autoencoder for video anomaly detection. In *Proceedings of the 25th ACM international conference on Multimedia*, pages 1933–1941, 2017. 3
- [64] Bo Zong, Qi Song, Martin Renqiang Min, Wei Cheng, Cristian Lumezanu, Daeki Cho, and Haifeng Chen. Deep autoencoding gaussian mixture model for unsupervised anomaly detection. In *International conference on learning representations*, 2018. 3
- [65] Yang Zou, Jongheon Jeong, Latha Pemula, Dongqing Zhang, and Onkar Dabeer. Spot-the-difference self-supervised pre-training for anomaly detection and segmentation. In *Computer Vision–ECCV 2022: 17th European Conference, Tel Aviv, Israel, October 23–27, 2022, Proceedings, Part XXX*, pages 392–408. Springer, 2022. 6